

# Assimilation of Doppler radar Data with WRF 4DVAR for a Convective Case

<sup>1</sup>Y.-R. Guo, <sup>1</sup>J. Sun, <sup>2</sup>E. Lim, <sup>1</sup>X.-Y. Huang, <sup>1</sup>X. Zhang, <sup>3</sup>S. Sugimoto

<sup>1</sup>National Center for Atmospheric Research  
P. O. Box 3000, Boulder, CO 80307, USA

<sup>2</sup>Korean Meteorological Administration  
Seoul, Korea

<sup>3</sup>Central Research Institute of Electric Power Industry  
Abiko, Japan

## Abstract

The 4DVAR component in WRF-VAR system has been developed for years. The prototype of this 4DVAR component, which is consistent with the WRF model but includes only simple physics packages, has been applied to different synoptic cases with rather larger scales. In order to examine the performance of the WRF 4DVAR on meso and convective scales and to improve the convective weather forecast, in this study, we used the WRF 4DVAR to assimilate multiple-radar data.

To better understand the performance of the WRF 4DVAR, first we conducted a set of experiments with the OSSE approach. The performance of the 4DVAR can be evaluated by verifying against the TRUTH. The results showed that the 4DVAR did much better job than the 3DVAR in terms of the hourly rainfall forecasts. Then, the real radar radial velocity and reflectivity from 10 NEXRAD sites for 13 June 2002 IHOP case are processed and assimilated with WRF-VAR system. From the threat scores of hourly rainfall forecast verified against the NCEP Stage IV data, the 4DVAR also outperformed over the 3DVAR and NCEP GFS analysis. This work demonstrated that now the WRF 4DVAR can be used as a tool in the convective-scale weather research. The major problem is that the computing efficiency still needs to be improved.

## 1. Introduction

Four-dimensional Variational Data Assimilation (4DVAR) is one of the powerful analysis systems in the Numerical Weather Prediction (NWP), which has been implemented in many operational centers, especially JMA have developed a 4DVAR system (JNoVA) for JMA nonhydrostatic model for mesoscale application (Honda et al, 2005). One of the advantages of 4DVAR is to use a forecast model as a constraint, which ensures the dynamic balance of the final analysis. To initialize the WRF model, the 4DVAR component of WRF-Var (WRF 4DVAR) has been under extensive development since 2004, and a series of experiments has been conducted for different synoptic cases with rather larger scales (Huang et al 2008).

As the WRF 4DVAR was continuously improved, it is possible to apply the system on meso and convective scales. In this study, we used the WRF 4DVAR to assimilate multiple-radar data from NEXRAD over the central United States for a convective system on 13 June 2002 that was observed during the IHOP experiment.

## 2. WRF 4DVAR System

A detailed description of WRF 4DVAR system can be found in Huang et al. 2008. It makes use of many pre-existing components of WRF 3DVAR, including observation operator, quality control, background error covariance, minimization inner-loop assuming Gaussian error covariance, and iterative outer loop to account for the effect of nonlinearities in the assimilation algorithm. In the outer loop, the full WRF nonlinear model is run to update the basic state from which the tangent linear model is derived. The tangent linear and the adjoint models are executed in the inner loop for the minimization. At present, the tangent linear and adjoint model include the full dynamics, a simple vertical diffusion scheme with surface friction, and a large-scale condensation scheme. More work is underway to add more physics to the inner loop.

The cost function is the summation of the three terms: the background term, the observation term, and the noise-controlled (digital filter) term. A number of variable transformations are operated to the model prognostic variables to precondition the cost function and to enforce balance constraints. Consequently, the control variables of the cost function are stream function, unbalanced velocity potential, unbalanced

temperature, pseudo relative humidity, and unbalanced surface pressure. The final analysis increment includes the x- and y-components of velocity, temperature, water vapor mixing ratio, and surface pressure.

For radar data assimilation, a number of modifications were made (Xiao et al. 2005, 2007). First, vertical velocity increment is added to the analysis variables via the Richardson balance equation, which combines the continuity equation, adiabatic thermodynamic equation, and hydrostatic relation. Second, the total water is used as the moisture control variable, instead of the pseudo relative humidity, for the assimilation of radar reflectivity. The partitioning of the total water into water vapor, cloud water, and rainwater is then achieved by using a warm-rain parameterization scheme. Lastly, the observation operators for assimilating Doppler radar radial velocity and reflectivity are developed.

### 3. Overview of IHOP 12-13 June 2002 case

Several convective systems occurred during June 12 and 13 2002 in the IHOP domain. This study focuses on the squall line initiated east of a triple point (intersection of an outflow and a dryline; marked by "T" in Fig. 1a) near the Oklahoma-Kansas border around 2100 UTC and propagated southeastward. Fig. 1 shows the convective activity at two different times by the merged reflectivity field at 0.5° elevation angle from multiple WSR-88D radars and NCAR's S-Pol (S-band dual-polarization Doppler radar). The merging of the radar reflectivity was done by choosing the maximum reflectivity at each grid point from data values given by different radars. A composite map of surface wind observations (white barbs) from several surface networks is overlaid. The blue wind barbs are surface observations from the METAR (METeorological Aerodrome Reports) stations. The radar locations are marked by the radars' names in red letters. Several mesoscale boundaries, including a nearly stationary outflow boundary from previous day convection (orange broken line in Fig. 1a), a dry line (pink line), and a weak cold front (brown line), are observed. A mesoscale circulation (mesoscale low) around the triple point is evidently shown by the surface observations. The warm, moist air mass to the east of the dryline and south of the outflow boundary contained CAPE near 2000 J kg<sup>-1</sup> and little CIN (convective inhibition) around 2100 UTC. The air mass to the north of the outflow boundary is slightly cooler.

Convective cells are developing east of the triple point and are clearly visible at 2120 UTC (Fig. 1a). The thunderstorm near the triple point intensified and new storms were developed near the Oklahoma-Kansas

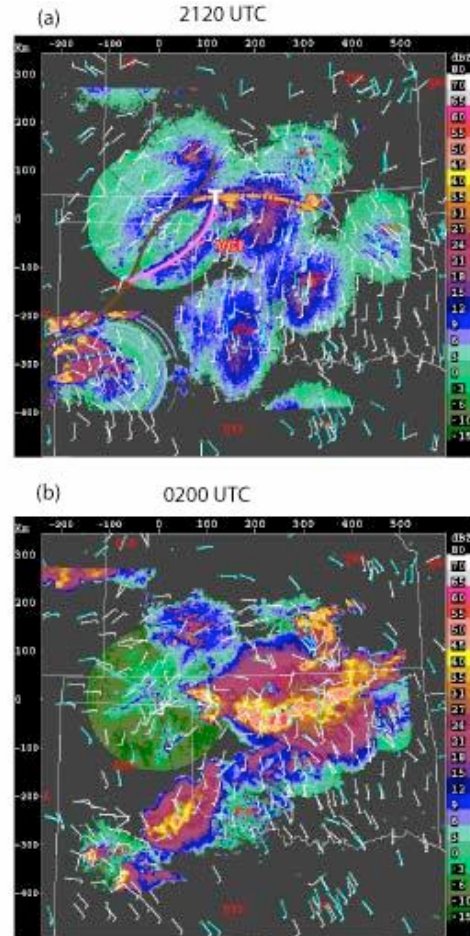


Fig. 1 Merged radar reflectivity image using the 0.5° elevation angle data at 2120 UTC (a) and 0200 UTC (b). The surface wind from METAR is shown by cyan wind barb and from a composite of all surface networks is shown by white. The cold front (brown line), dryline (pink line), and outflow boundary (dashed orange) are depicted in (a).

border as the circulation associated with the mesoscale low strengthened. Damaging winds and large hail were reported in conjunction with some of the storms. The severe storm near the triple point produced golf-ball-size hail, maximum outflow wind speeds exceeding 30 m/s, flashing flood, and at least one tornado. By 0200 UTC, a well-organized squall line had developed (Fig. 1b) and it then moved southeastward. The squall line is reduced in spatial extension at 0400 UTC and completely dissipated around 0900 UTC. The stage-IV precipitation analysis of the National Centers for Environmental Prediction reported a maximum hourly rainfall of 57.8 mm at 0200 UTC in north Oklahoma. Our focus in the current study is not on the prediction of the initial storm development, but the prediction of

evolution of existing storms and development of new ones from outflow interaction.

The radar data preprocessing quality control follows closely the procedure in VDRAS (Sun 2005b). It includes interpolating data from radar spherical coordinates to uniformly gridded data on elevation angle surfaces, noise removal, velocity unfolding, void filling, and superobbing, and estimation of observation errors.

#### 4. OSSE Experiment and results

##### a, Control run and simulated radar data

For OSSE (Observing System Simulation Experiment), the mimic radial velocity and reflectivity data from a control simulation are used as *truth*. This control simulation is a 12/4-km nested domain 24-h forecast, initiated at 1200 UTC on 12 June using AWIP 40 km analysis (Fig.2). The physics options include the Thompson microphysics (Thompson et al. 2004), Noah land surface model, and Yonsei University boundary layer scheme.

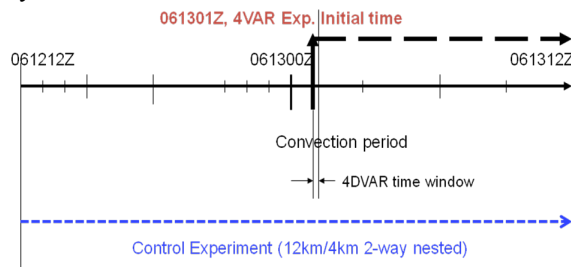


Fig. 2 The schematic diagram for OSSE Experiments.

The 4-km control simulation domain and the data assimilation (DA) experimental domain are shown in Fig. 3. A smaller domain was chosen for DA Experiments because of the computer resource limitation for WRF 4DVAR. The initial time for all DA Experiments is 0100 UTC 13 June, i.e. 13-h forecast from the control run. There are 10 radars in or near the 4DVAR domain, each located at the actual site of the NEXRAD network (Fig. 5a). Four time periods of radar velocity and reflectivity data at 0100, 0105, 0110, and 0115 UTC 13 June were computed using the forecast data from the control simulation based on the following relationships, respectively:

$$V_r = \frac{1}{R} [(x_d - x_r)u + (y_d - y_r)v + (z_d - z_r)(w - V_t)]$$

$$Z = 43.1 + 17.5 \log(\rho q_r)$$

We also assume that both the radial velocity and reflectivity are available only at the grid points where the reflectivity is greater than 5 dBZ and there are no data above the 20° elevation angle and beyond 200km from each of radar sites.

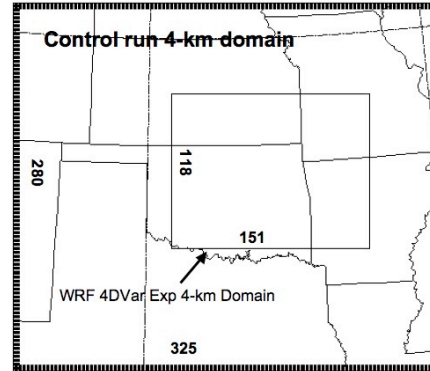


Fig. 3 The 4km domain of the control simulation and the 4DVAR data assimilation domain. The numbers show the grid points on each domain.

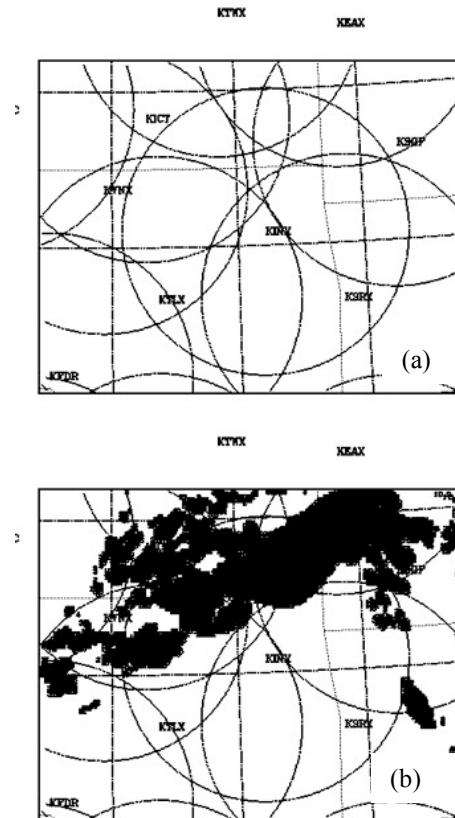


Fig. 4 (a) The over the DA Experimental domain; (b) The radar data coverage at 0100 UTC 13 June 2002.

Fig. 4a shows the radar location and the 200km ring for each radar. Fig.4b shows the data coverage at 0100 UTC 13 June 2002.

*b, Experiment design*

Four forecasting experiments are performed, and two of them conducted radar data assimilation (see Table 1). Note that the data assimilation experiments only used radial velocity data but not the reflectivity data.

Table. 1 OSSE Experiment design

Exp.	description
TRUTH	Initial condition from the control simulation and boundary condition from NCEP GFS data
NODA	Both initial condition and boundary condition from NCEP GFS data.
3DVAR	analysis at 2002061301Z, and boundary condition from NCEP GFS. Only Radar radial velocity at 2002061301Z is assimilated (total # of data points = 65,195).
4DVAR	Initial condition from a 4DVAR analysis at 2002061301Z, and boundary condition from NCEP GFS. The radar radial velocity at 4 times, 200206130100, 05, 10, and 15, are assimilated within the 15 min window (total # of data points = 262,445).

In both the 3DVAR and 4DVAR experiments, the background error statistics (BES) are obtained by interpolation from a 12-km resolution BES for IHOP case. The first guess is NCEP GFS analysis. The number of iterations for the 3DVar is 67, and for 4DVAR is 60.

*c, Results*

Fig. 5 shows the 3-hour forecasts of hourly-accumulated precipitation from the four experiments. The forecast that is initialized by the 4DVAR radar data assimilation produces the precipitation band that is in better agreement with the truth than the other two experiments. The 1h forecasts (not shown) indicate that both the NODA and 3DVAR experiments do not produce any precipitation due to spin-up. The analysis increment (not shown) of the temperature field suggests that the 4DVAR experiment results in better temperature retrieval than 3DVAR.

The quality of the rainfall forecast is evaluated and compared by computing the threat score. The result is

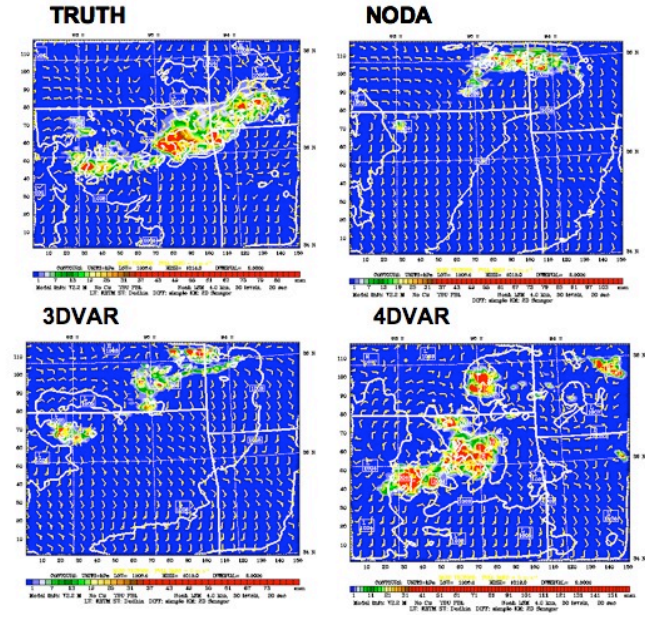


Fig. 5 3h forecasts, starting at 0100 UTC, 12 June, of hourly-accumulated precipitation from TRUTH, NODA, 3DVAR, and 4DVAR of the OSSEs.

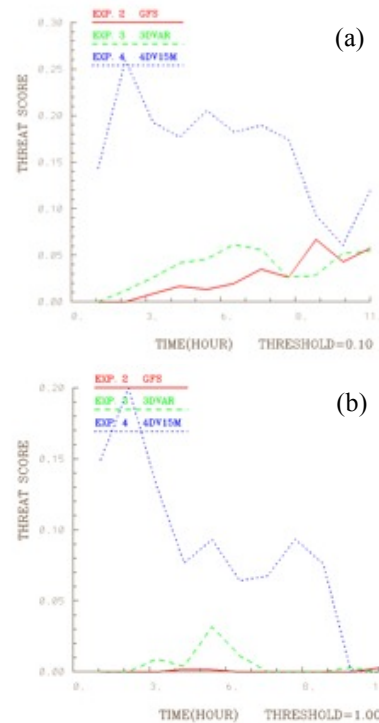


Fig. 6 Threat score of hourly precipitation with respect to forecast hour for thresholds of (a) 0.1 cm and (b) 1.0 cm from the OSSEs.

shown in Fig. 6. It clearly shows that 4DVAR produces significantly improved forecasts for both threshold of 0.1cm and 1cm hourly-accumulated rainfall. In compared the scores from 3DVAR with those from

GFS (NIODA), however, it only gave minor improvement of the precipitation forecast skill.

## 5. Real data experiments

### a) Experiment design

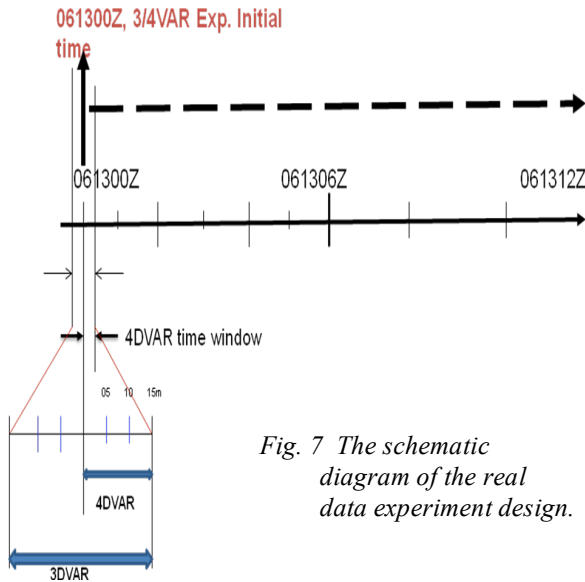


Fig. 7 The schematic diagram of the real data experiment design.

The real data assimilation experiments are performed on the same domain as the OSSE, but initiated at 0000 UTC, 13 June, which is 1 hour earlier than that for OSSE (Fig. 7). The reason to choose 0000 UTC as the initial time is that more conventional data (soundings, etc.) will be available for DA experiments. The real data experiments also include four experiments, NODA, 3DVARA, 4DVAR, and 4DVARA. The experiments NODA and 4DVAR are similar to their counterparts of the OSSEs except that real data are used. The experiments 3DVARA and 4DVARA are similar to 3DVAR and 4DVAR but assimilate not only radar radial velocity but also conventional observations.

### b) Results

Fig. 8 shows the 4-hour forecasts of hourly precipitation from the four real-data experiments. 4DVAR produces the precipitation band that agrees quite well with the observation except that it propagates faster toward the southeast. One surprising result, which is different from OSSE, is that the 3DVAR yields poorer forecast than NODA. This may be caused by several factors.

(i) The WRF forecast model is not perfect. In OSSE, the *TRUTH* and forecasts are generated by the

same WRF forecast model, which was known as the *identical twin* problem, and usually gave an optimistic conclusion;

(ii) The distribution of radar radial velocity data in OSSE and real observations is different because the simulated convection and real convection are different. Furthermore, the observation errors of radial velocity are always specified to 1 m/s for OSSE, but for real data, the observation errors are specified by radar data processing procedure (Sun 2005);

(iii) The performance of a 3DVAR system is mostly determined by background error statistics (BES) definition. Here, the BES for our 4-km resolution 31-level experimental domain was obtained by interpolation from the BES for a 12-km resolution 35-level domain, not derived from the forecast data from our model domain. This BES may not be suitable for our situation. In the 4DVAR, the BES may not be as critical as in the 3DVAR because the 4DVAR included the forecast model forward integration and adjoint model backward integration during the minimization process.

We are in the process of investigating the causes.

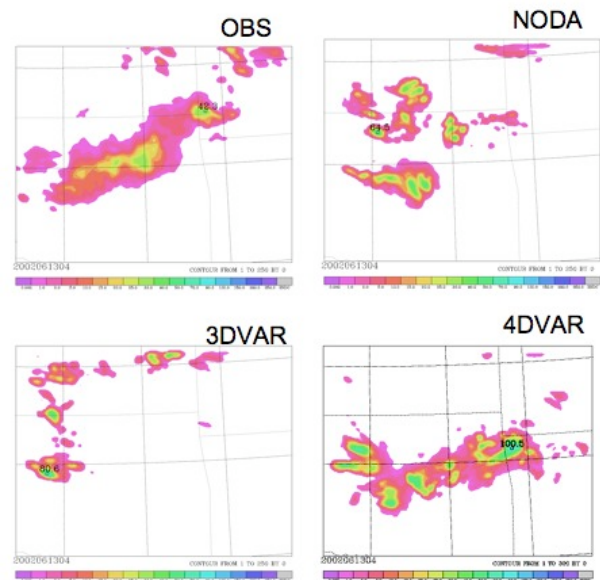


Fig. 8 The hourly precipitation forecast ending at 0400 UTC 13 June (4-h forecasts) from NODA, 3DVARA, and 4DVAR of the real data experiments.

The quality of the precipitation forecasts is also evaluated by computing the threat score. Fig. 9 shows

the result. In average, both 4DVAR and 4DVARA improve the threat scores at most of the forecast times over NODA and 3DVARA.

With the threshold of 0.1 cm, 4DVARA (with the conventional data) is better than 4DVAR (without conventional data) for the first 9-h forecast. But with the threshold of 0.5 cm, 4DVAR is better than 4DVARA. It is still a challenge how to better use the conventional data for the convection forecast. It is interesting that the forecasts at some hours (6- and 7-h in Fig. 9a and 3- and 4-h in Fig.9b), the NODA gave better forecast skills. The initial state for NODA is from AWIP 40-km analysis, which may correctly describe the larger scale atmospheric state already. A mesoscale data assimilation system should not destroy the larger scale features, and introduce the smaller scale details correctly. It may not be an easy job.

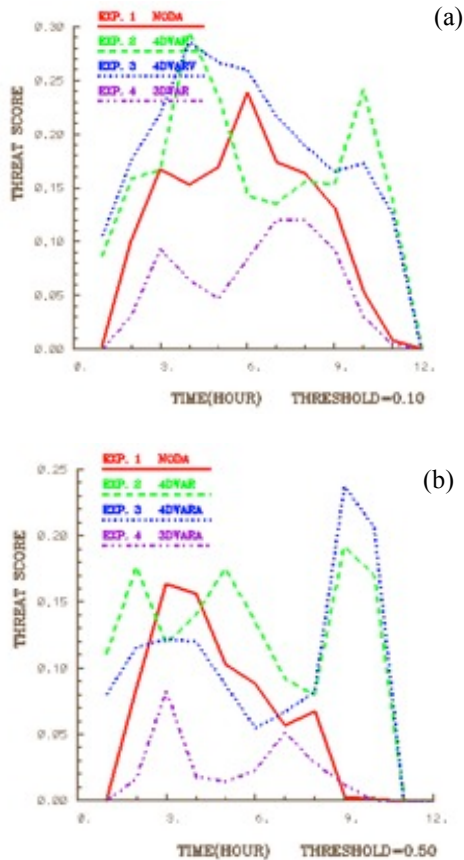


Fig. 9 Threat score of hourly precipitation with respect to forecast hour for thresholds of (a) 0.1 cm and (b) 0.5 cm from the real radar data assimilation.

## 6. Summary and conclusions

OSSE and real data experiments are performed to examine the feasibility and impact of assimilating Doppler radar radial velocity on forecasting of severe convective weather. A case of squall line that occurred during the IHOP experiment is used for the study. Both the OSSE and the real data experiments show that the assimilation of radial velocity using WRF 4DVAR improves the short-term precipitation forecasts over WRF 3DVAR and the experiments that do not have radar data assimilation. At this stage, the WRF 4DVAR can be used as a tool in the convective-scale weather research. Work is still in progress to examine the sensitivity of the 4DVAR analysis and forecast with respect to assimilation window.

In terms of assimilation of radar reflectivity, the partitioning of total water may not be necessary for 4DVAR because the cloud water and rain water will be the model prognostic variables. Currently, however, the cloud water and rain water are not the control variables, and the incremental approach is implemented in WRFVar system. So in order to assimilate the reflectivity data, but not using a partitioning algorithm, the outer loops must be used in WRF 4DVAR for the cloud and rain water adjustment. This is another research topic for radar data assimilation with WRFVar.

## 7. Acknowledgement

This study is sponsored the Central Research Institute of Electrical Power Industry (CRIEPI) of Japan. The authors wish to thank Hongli Wang and Yunsheng Chen for software engineering support on this work.

## References

- Honda, Y., M. Nishijima, K. Koizumi, Y. Ohta, K. Tamiya, T. Kawabata and T. Tsuyuki, 005: A pre-operational variational data assimilation system for a non-hydrostatic model at the Japan Meteorological Agency: Formulation and preliminary results. *Q. J. R. Meteorol. Soc.*, 131, 3465-3475.
- Huang X., Q. Xiao, D. M. Barker, X. Zhang, J. Michalakes, W. Huang, T. Henderson, J. Bray, Y. Chen, Z. Ma, J. Dudhia, Y. Guo, X. Zhang, D-J Won, H-C Lin, Y-H Kuo, 2008: Four-dimensional variational data assimilation for WRF: formulation and preliminary results. Submitted to *Mon. Wea. Rev.*

- Sun, J., 2005: Convective-scale assimilation of radar data: progress and challenges. *Q. J. R. Meteorol. Soc.*, *131*, 3439-3463.
- Thompson, G., R. M. Rasmussen, and K. Manning, 2004: Explicit forecasts of winter precipitation using an improved bulk microphysics scheme. Part I: Description and sensitivity analysis. *Mon. Wea. Rev.*, *132*, 519-542.
- Xiao, Q., Y.-H. Kuo, J. Sun, W.-C. Lee, E. Lim, Y. Guo, D. M. Barker, 2005: Assimilation of Doppler radar observations with a regional 3D-Var system: impact of Doppler velocities on forecasts of a heavy rainfall case. *J. Appl. Meteor.* **44**, 768-788.
- Xiao, Q., Y.-H. Kuo, J. Sun, W.-C. Lee, and D. Barker, 2007: An Approach of Doppler Reflectivity Data Assimilation and its Assessment with the Inland QPF of Typhoon Rusa (2002) at Landfall, *J. Appl. Meteor.*, *46*, 14-22.